Sinopfbd, 2024; 9(1): 44-60 **https://doi.org/10.33484/sinopfbd.1369460**

Sinop Üniversitesi Fen Bilimleri Dergisi
Sinop Uni J Nat Sci
E-ISSN: 2564-7873

https://dergipark.org.tr/tr/pub/sinopfbd

The Effect of Deposition Temperature on Structural, Morphological, and Dielectric Properties of Yttria-Doped Zirconia Thin Films

Şerif RÜZGAR[1] and Veysel ERATİLLA[2]

How to cite: Rüzgar, Ş., & Eratilla, V. (2024). The effect of deposition temperature on structural, morphological, and dielectric properties of yttria-doped zirconia thin films. *Sinop Üniversitesi Fen Bilimleri Dergisi*, *9*(1), 44-60. https://doi.org/10.33484/sinopfbd.1369460

Research Article

Corresponding Author
Şerif RÜZGAR
serif.ruzgar@batman.edu.tr

ORCID of the Authors
Ş.R: 0000-0002-4964-2202
V.E: 0000-0002-3511-5612

Received: 01.10.2023
Accepted: 13.02.2024

Abstract

The aim of this study was to investigate the effect of deposition temperature on the structural, optical, morphological, and dielectric properties of yttria-stabilised zirconia (YSZ) films prepared by sol-gel spin-coating method. X-ray diffraction (XRD) measurements of YSZ films showed that the peaks of the cubic phase were prominent and the peak intensities increased with deposition temperature. The crystallite size, dislocation density, and microstrain of the thin films were identified by XRD. It was observed that the crystal size of the YSZ thin films increased from 16 nm to 22 nm with the deposition temperature. The surface roughness of the thin films was found to have changed as revealed by Atomic Force Microscopy (AFM) measurements. The roughness increased from 7.72 nm to 11.92 nm with increasing temperature. The optical transmittance of the YSZ thin films was investigated in the wavelength range 200-900 nm and was found to increase slightly with increasing deposition temperature. Metal-Oxide-Semiconductor (MOS) devices were fabricated from these YSZ materials for dielectric characterization. The dielectric properties of the Ag/YSZ/n-Si MOS structure were investigated. It was found that the capacitance, conductivity and other dielectric parameters of these structures are strongly frequency dependent.

Keywords: Yttrium stabilized zirconia, MOS, dielectrics, annealing effect, sol gel

Biriktirme Sıcaklığının İtriyum Katkılı Zirkonya İnce Filmlerin Yapısal, Morfolojik ve Dielektrik Özelliklerine Etkisi

[1]Department of Opticianry Program, Vocational School of Health Services, Batman University, Batman, Turkey

[2]Faculty of Dentistry, Prosthetic Dentistry Department, Batman University, Batman, Turkey

Öz

Bu çalışmanın amacı, sol-gel spin-kaplama yöntemiyle hazırlanan itriya ile stabilize edilmiş zirkonya (YSZ) filmlerin yapısal, optik, morfolojik ve dielektrik özelliklerine biriktirme sıcaklığının etkisini araştırmaktır. YSZ filmlerinin X-ışını kırınımı (XRD) ölçümleri, kübik fazın tepe noktalarının belirgin olduğunu ve tepe yoğunluklarının biriktirme sıcaklığıyla birlikte arttığını gösterdi. İnce filmlerin kristalit boyutu, dislokasyon yoğunluğu ve mikro gerilimi XRD ile belirlendi. YSZ ince filmlerinin kristal boyutunun biriktirme sıcaklığıyla birlikte 16 nm'den 22 nm'ye arttığı gözlendi. Atomik Kuvvet Mikroskobu (AFM) ölçümleri sonucunda ince filmlerin yüzey pürüzlülüğünün değiştiği tespit edildi. Artan sıcaklıkla pürüzlülük 7.72 nm'den 11.92 nm'ye yükseldi. YSZ ince filmlerinin optik geçirgenliği 200-900 nm dalga boyu aralığında araştırılmış ve artan biriktirme sıcaklığıyla birlikte hafifçe arttığı

bulunmuştur. Dielektrik karakterizasyonu için bu YSZ malzemelerinden Metal Oksit-Yarı İletken (MOS) cihazlar üretildi. Ag/YSZ/n-Si MOS yapısının dielektrik özellikleri araştırıldı. Bu yapıların kapasitans, iletkenlik ve diğer dielektrik parametrelerinin güçlü bir şekilde frekansa bağlı olduğu bulunmuştur.

Anahtar Kelimeler: İtriyum stabilize zirkonya, MOS, dielektrikler, tavlama etkisi, sol jel

Introduction

Zirconium dioxide, also known as zirconia (ZrO2), was first discovered in 1789 [1]. Zirconia films possess a number of exceptional properties that give them an important role in both theoretical research and real-world applications. Due to its chemical stability, high dielectric constant, high degree of transparency in the ultraviolet and visible spectrum, high forbidden optical band gap, high melting point, high hardness and good thermal insulation properties, this versatile material can be used for a number of practical applications such as thermal and chemical barriers, as buffer layers for growing high-temperature superconducting films and as sensors in microelectronics [2-5]. Traditionally, zirconia has been doped with many metal oxides such as Y2O3, CaO, La2O3, MgO and Ce2O3 [6]. Typically, these oxides are doped to maintain zirconia in its tetragonal or cubic phase at low temperatures [6]. Among these oxides, yttrium oxide, when doped into the zirconia material, also imparts various properties to the host material. Some of these benefits can be listed as follows: Improved mechanical properties: The addition of yttria to zirconia can significantly improve its mechanical properties, including strength, toughness, and fracture resistance. This is due to the formation of a uniform and fine-grained microstructure, which can prevent crack propagation and increase corrosion resistance [7]. A high melting point and high thermal shock resistance make yttrium-stabilized zirconia ideal for high temperature applications such as solid oxide fuel cells, catalysis, and thermal barrier coatings [8]. YSZ is a potential material for use in oxygen sensors due to its high oxygen ion conductivity [9]. Due to its superior biocompatibility, low toxicity, and corrosion resistance, YSZ has been extensively researched for its potential application in dental and orthopedic implants [10, 11]. In addition, it is extensively used in implantology, orthodontics, restorative dentistry and prosthodontics, which are all sub-disciplines of dentistry, to improve the infrastructure of post-core material and crown-bridge restorations [12, 13]. Consequently, YSZ stands out as one of the popular solid electrolytes used in a variety of electrochemical devices such as gas sensors and oxygen membranes [14]. Apart from these devices, MOS structures in which YSZ films can be used as applications also attract attention with their extraordinary features. The MOS structure has been a widely adopted technology for several decades. Due to the interface effect of metal-oxide and oxide-semiconductor, this MOS device is primarily utilized for diodes and MOS capacitors in integrated circuits, particularly photodiodes [15, 16]. Furthermore, MOS structures are suitable for energy storage devices due to the dielectric property of the oxide layer [17]. It is possible to create high-quality YSZ oxides utilizing a range of physical and chemical methods. These techniques include atomic layer deposition [18], laser-assisted plasma coating

[19], power impulse magnetron sputtering [20], chemical vapor deposition [21] and the sol-gel method [22, 23]. Among these methods, sol-gel offers several advantages over other deposition techniques, including: uniformity and control, which allows for precise control over the thickness and composition of the deposited films, low temperature processing, high purity, versatility, cost effectiveness, which is relatively inexpensive compared to other deposition techniques [24-26]. The aim of this study is to investigate the influence of deposition temperature on the properties of YSZ thin films and to explore the underlying mechanisms that control their growth and material properties. The results of this investigation will provide insight into the structure-property relationships of YSZ thin films and facilitate the optimization of their performance for various applications. Ultimately, a better understanding of the effect of deposition temperature on YSZ thin films will enable the production of high quality YSZ thin films with desired properties.

Experimental

In this study, the sol-gel technique was used to deposit thin films. Zirconyl chloride octahydrate (sigma-aldrich) and yttrium (III) nitrate hexahydrate (sigma-aldrich) were employed as starting materials for the synthesis of YSZ thin films. YSZ precursors of 0.1 M were prepared by dissolving zirconium oxychloride octahydrate and yttrium (III) nitrate hexahydrate in 2-methoxyethanol solvent with monoethanolamine stabilizer. The yttrium ratio in the ZrO2 solution was adjusted to 7% of the atomic weight of the zirconium metal. The prepared solution was stirred at 60°C for 2 hours to obtain a transparent liquid. Prior to the formal coating process, the precursor liquid was filtered through a 0.22 μm injection filter. Prior to thin film deposition, Si and quartz substrates were cleaned using RCA (Radio Corporation of America) cleaning techniques. In addition to this cleaning, n-Si substrates were immersed in 1% HF solution and the natural SiO2 on the surface was removed. Finally, the n-Si and quartz substrates were rinsed with deionized water and dried with N_2 gas to obtain a hydrophilic surface. YSZ films were grown on n-Si and quartz substrates at room temperature for 30 s at 3000 rpm. After each deposition, the films were pre-annealed in an oven at 300°C and this process was repeated 10 times. Finally, YSZ films were annealed for 2 hours at 700°C, 900°C, and 1100°C, respectively. These films were designated as YSZ7 (annealed at 700°C), YSZ9 (annealed at 900°C) and YSZ11 (annealed at 1100°C) respectively. The thicknesses of YSZ7, YSZ9, and YSZ11 films were determined by atomic force microscopy to be 220 nm, 120 nm, and 95 nm, respectively. The schematic diagram of the YSZ/n-Si MOS structure, which was fabricated to examine the capacitance properties of the produced thin films, is shown in Figure 1. In order to perform the electrical characterization of the produced MOS structures, silver paste contacts were made on the films. The resistivity of commercially purchased silver paste is 1.59 μΩ-cm. The C-V characterization of the structures was carried out using the Keithley 4200 semiconductor characterization system. Optical, crystallographic and surface properties of thin films

were investigated using Shimadzu UV-19, Rigaku Miniflex II, and Park System XE-100 Atomic Power Microscope, respectively.

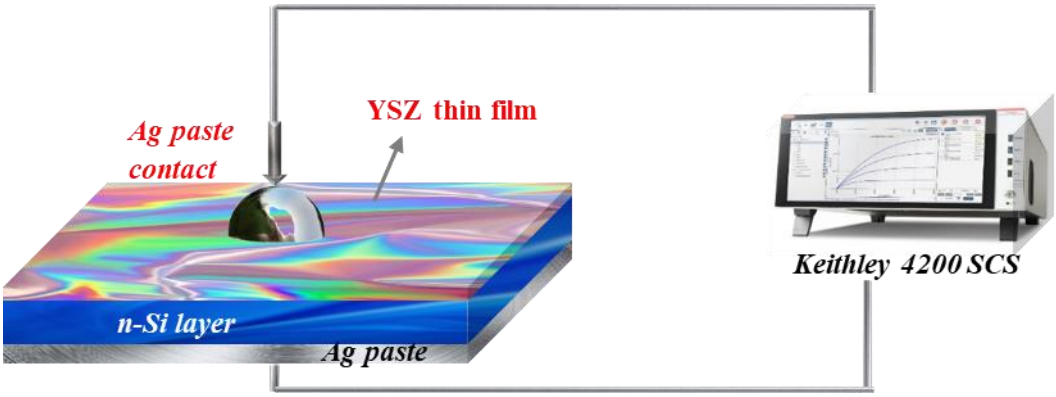

Figure 1. *The schematic diagram of YSZ/n-Si MOS structure*

Result and Discussions

The crystallinity and preferred crystal orientation of the YSZ films were determined through the XRD technique. Figure 2 shows the XRD patterns of YSZ thin films formed on n-Si substrates at 0.1 M with varying deposition temperature and the photograph of the YSZ thin films deposited on n-Si wafers. The cubic crystal structure is confirmed by the four prominent peaks corresponding to (111), (200), (220) and (311) planes in all YSZ thin film samples [27-29]. No impurity peaks are visible either, all of these polycrystalline ZrO2 films are free of impurities. The intensity of the most prominent (111) reflection is observed to increase with increasing deposition temperature, indicating that the improvement in crystal quality of YSZ is caused by the increase in temperature. The (200), (220), and (311) orientations are the other orientations observed with slightly lower intensities. The average crystal size of the nanostructured YSZ films is calculated by the semi-empirical Debye-Scherrer formula [24]:

$$D = \frac{0.9\lambda}{\beta \cos\theta} \quad (1)$$

where D, λ, θ, and β are the mean crystal size, the applied X-ray wavelength, the diffraction angle in degrees and the full width at half maximum (FWHM) of the observed diffraction peak in radians, respectively. The D values for YSZ films were calculated to be 16 nm, 19 nm and 22 nm for YSZ7, YSZ9 and YSZ11 films from AFM micrographs, respectively. The increase in crystallite size with increasing temperature can be explained by the coalescence of smaller crystallites into larger ones. During this process, elevated temperatures can induce grain boundary migration leading to the growth of larger grains [30-32].

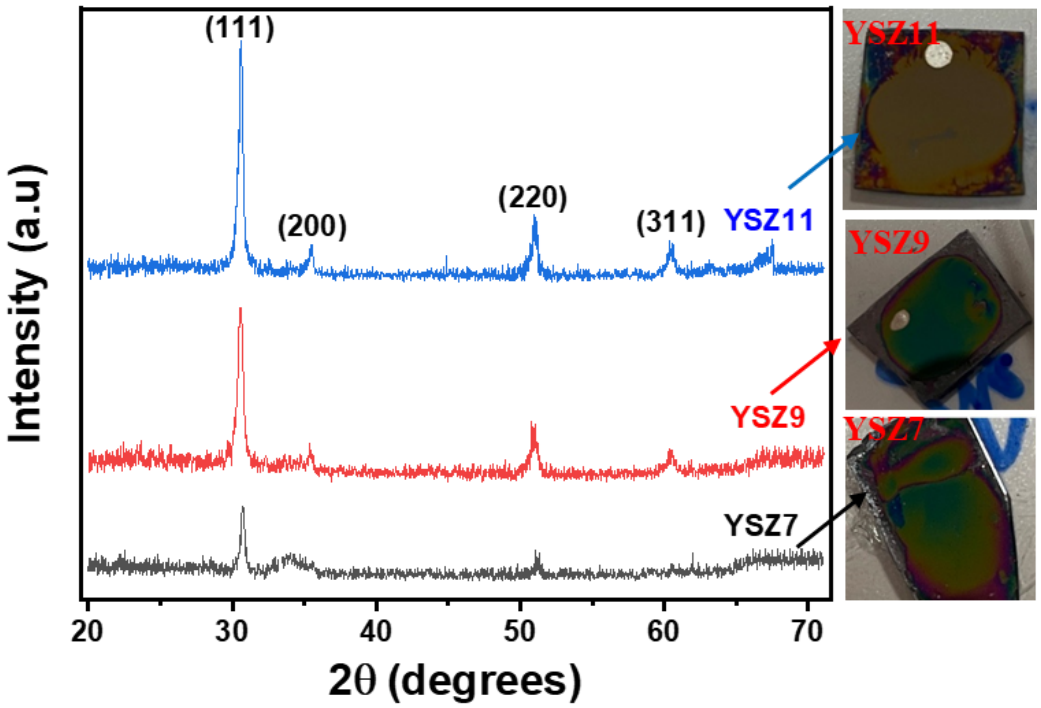

Figure 2. *The XRD patterns of YSZ thin films and the photograph of the YSZ thin films coated on n-Si wafers*

The improved crystallinity is achieved by annealing, which allows the atoms of the film to rearrange into a more ordered structure. In addition, it has been hypothesized that annealing films can reduce residual stress and a defect in the lattice structure, which would increase the growth rate [28, 33]. Other important parameters of crystal structures are dislocation density (δ), which is a measure of the number of dislocations (line defects) present in a crystal structure, and microstrain (ε), which is a measure of the degree of elastic deformation or strain within a crystal structure. These parameters can be defined by the following equations [27];

$$Dislocation\ density\ (\delta) = \frac{1}{D^2} \quad (2)$$

$$Micro\ strain\ (\varepsilon) = \frac{\beta \cos\theta}{4} \quad (3)$$

The D, δ, and ε values of the thin films are given in Table 1. From the observations, it can be concluded that changing the annealing temperature for YSZ thin films causes changes in the recrystallization process and parameters.

Table 1. *Crystallite size, dislocation density and micro strain of YSZ thin films obtained at different deposition temperature*

Sample	Crystallite Size, D (nm)	Dislocation Density, δ (10^{14} m^{-1})	Micro strain, ε (10^{-4})
YSZ7	16	40	22
YSZ9	19	29	18
YSZ11	22	21	16

The effect of annealing temperature on the surface morphology of YSZ films was investigated using AFM. Figure 3 shows the AFM images of the films.

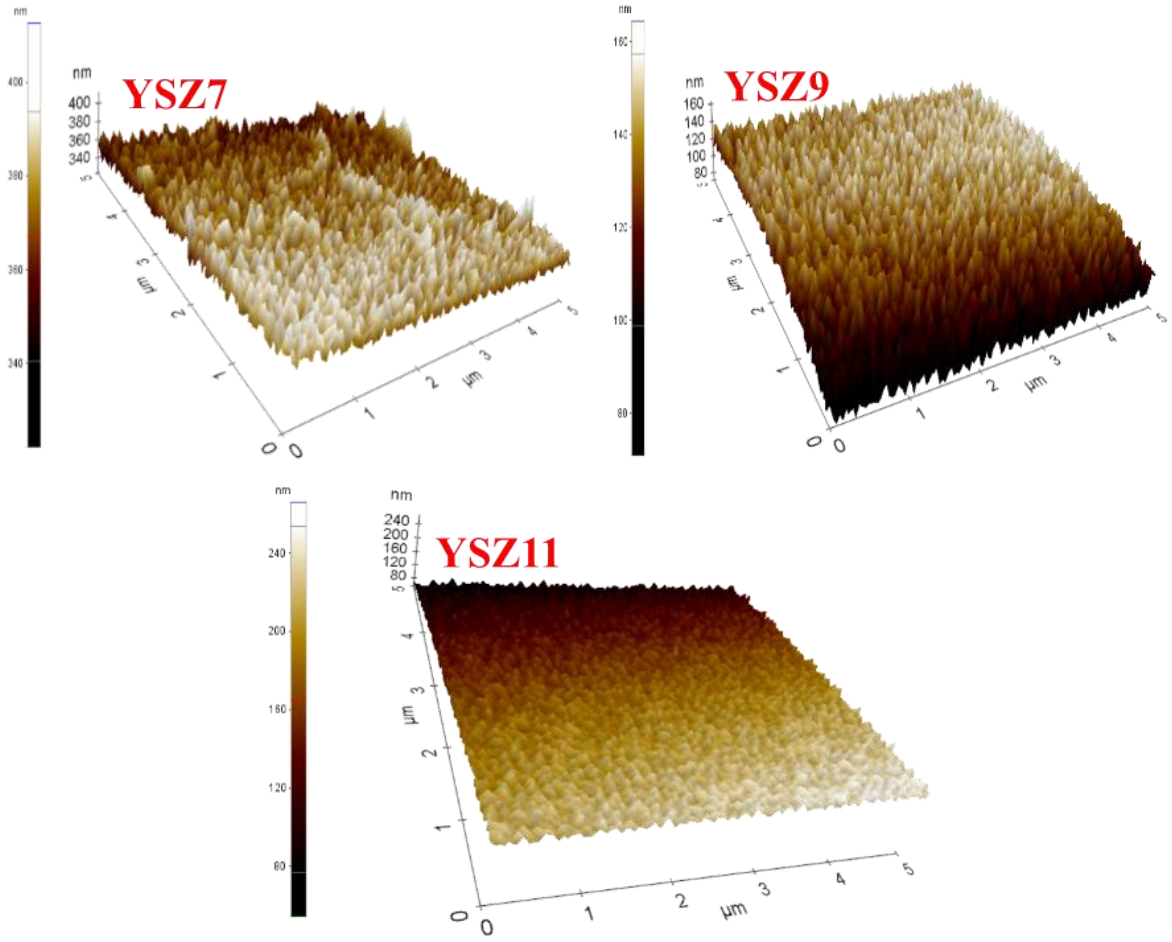

Figure 3. *The AFM images of YSZ thin films*

The surface roughness values for YSZ7, YSZ9 and YSZ11 films are 7.72 nm, 10.25 nm and 11.92 nm respectively. The AFM results showed that rougher films were formed with increasing growth temperature. The increase in roughness of Al doped ZrO2 films with annealing temperature was also reported by Cai et al. [34]. The increased surface roughness associated with annealing at higher temperatures may be due to agglomeration phenomena caused by greater heat absorption or a possible

crystallization factor resulting in large grains [34, 35]. The optical properties of the YSZ thin films were investigated using transmittance analyses. Figure 4 shows the spectra as a function of wavelength obtained by using UV-Vis spectroscopy to define the transmittance spectra in the range 200-900 nm.

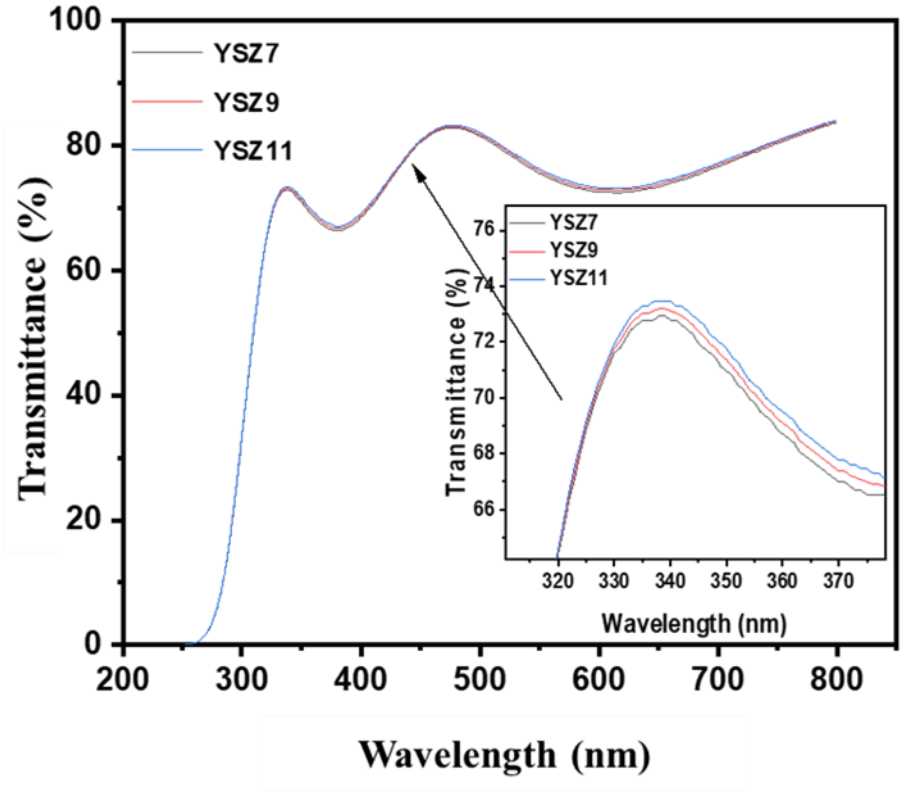

Figure 4. *The transmittance spectra of YSZ thin films. (Inset: Zoom of transmittance spectra)*

When the transmittance measurements of the YSZ films are examined, it can be seen that the thin films have a transmittance in the range of about 66-83%, and it can be seen from the inset graph that the transmittance increases slightly as the growth temperature increases. The transmittance of thin films can be influenced by several factors including the composition, thickness and microstructure of the film [36]. In general, increasing the deposition temperature can improve the crystallinity and reduce the defects in the thin film, leading to higher transmittance [37, 38]. Additionally, the optical transparency analysis of the films revealed slight interference fringes, which could be attributed to the homogeneity and smooth morphology of the thin films [39, 40]. The Tauc model was used to calculate the energy band gap (Eg) of YSZ films. The (ahυ)^2-hυ graphs of thin films are drawn and shown in Figure 5. It was observed from the graph that the optical band gaps of the thin films decreased as the deposition temperature increased. This situation is generally attributed to the quantum size effect [41, 42].

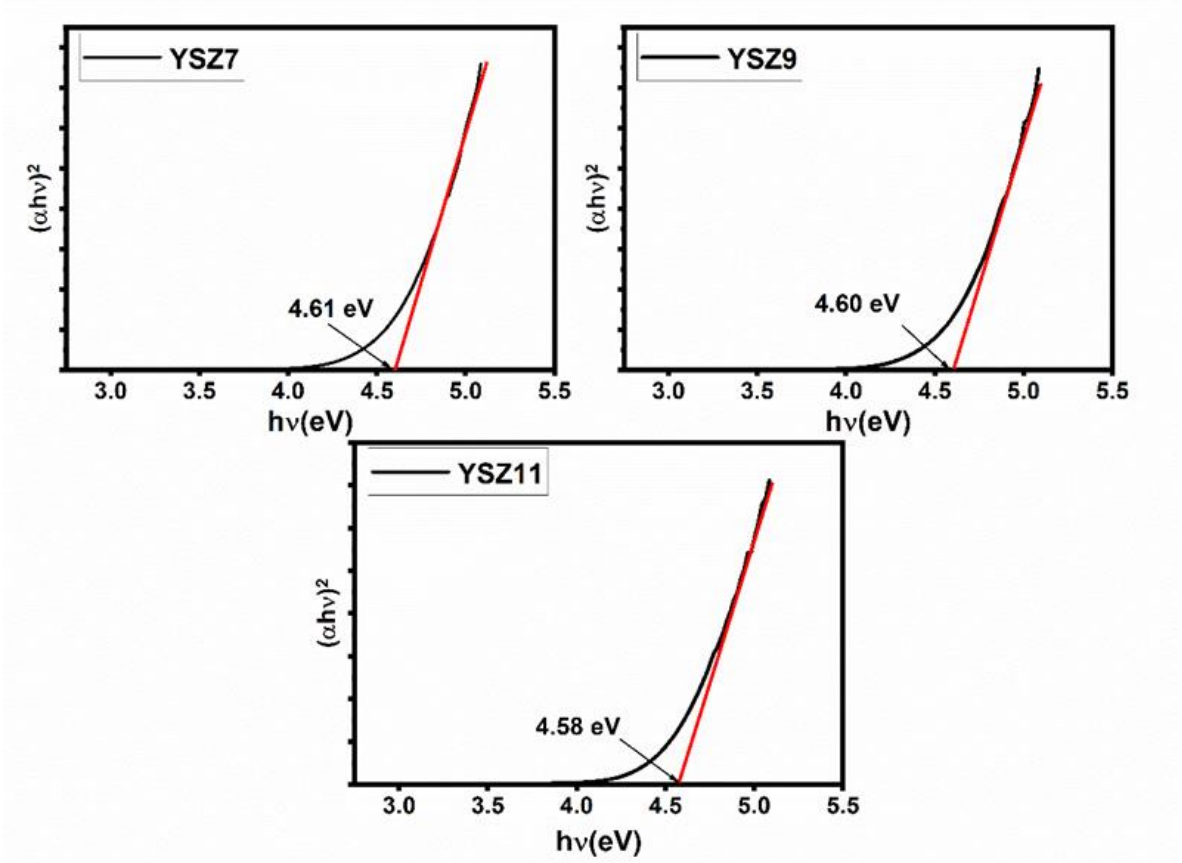

Figure 5. *Band gap prediction of YSZ thin films at various deposition temperatures using the Tauc method*

A dielectric is an insulator that can be polarized under an electric field. When subjected to an external electric field, electric charges within this dielectric material do not generate a current. However, the equilibrium positions of the charges change. As a result, the dielectric material becomes polarized and an electric field is generated within it. The external electric field is partially counteracted by the electric field within the material, which works towards equilibrium. This internal electric field persists, particularly in metals, until the applied external electric field is zeroed. Although the term "insulator" commonly implies low electrical conductivity, the term "dielectric" is typically used to describe materials with a high polarization capability. This is expressed by a quantity called the dielectric constant [43, 44]. In order to investigate some basic physical properties of the fabricated Ag/YSZ/n-Si MOS capacitor, capacitance-frequency (C- log (ω)), and conductance-frequency (G- log (ω)) measurements were investigated in a wide frequency range at room temperature. The C- log (ω) and G- log (ω) plots of the Ag/YSZ/n-Si structure is shown in Figure 6(a) and (b), respectively. The C- log (ω) plot for the fabricated structures is shown in Figure 6(a). According to this graph, the capacitance value decreases with increasing frequency and then reaches a constant value towards higher frequencies. This phenomenon is caused by the ability of the charge carriers to follow the AC signal. The contribution to the capacitance is limited because the charges at the states/traps cannot follow the AC signal at higher frequencies [45]. Upon examining the measurements of the fabricated MOS structures, it was observed

that the conductivity remained relatively unchanged up to 100 kHz, and thereafter, it increased with the rising frequency. The interface states and the ability of the charges to relax with time may be the cause of the change in conductivity with increasing frequency [46, 47]. Figure 6(c) shows the series resistance versus frequency (Rs-log (ω)) curves of MOS's calculated from C-f and G-f values. When the Rs-log (ω) curves of the MOS are examined, it can be seen that the series resistance values decrease with increasing frequency and remain constant at high frequencies. The presence of fixed and mobile oxide charges, as well as trapped charges in the oxide forming the interface states, can be identified as the underlying cause of the observed series resistance behavior [46, 48]. The fact that the series resistance values at high frequencies remain constant with frequency suggests that the interface states may not be able to follow the AC signal at these frequencies [45]. The localized states at the interface and the thickness of the layer are the main contributing elements, and together they have a considerable impact on the interfacial layer's dielectric characteristics and the capacitive performance of the MOS. As the experimental C and G values may change with bias voltage and frequency, a thorough dielectric analysis of the observed capacitive and conductive nature is required to appropriately determine the dielectric characteristic of the MOS [49].

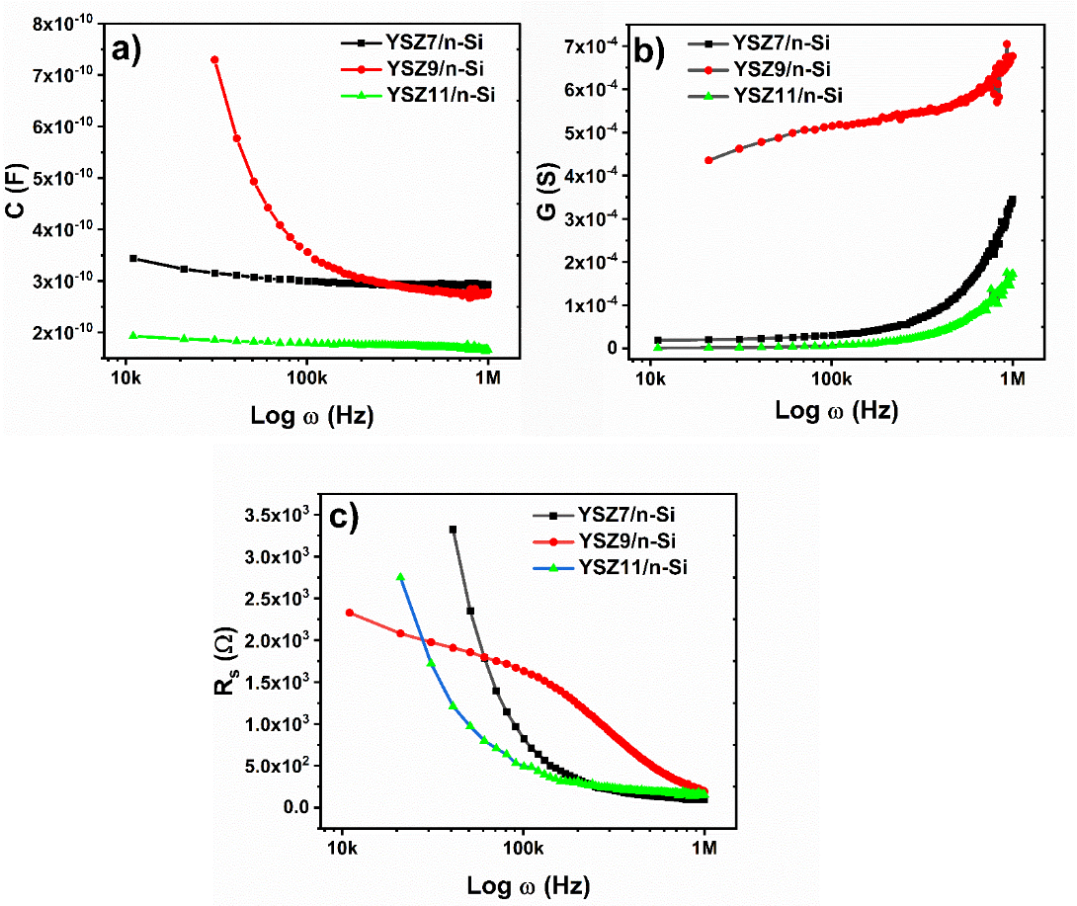

Figure 6. (a) *The plots of C- log (ω)* ***(b)*** *G- log (ω) and* ***(c)*** *Rs- log (ω) for Ag/YSZ/n-Si MOS structures*

In this situation, it is possible to evaluate the dielectric parameters complex dielectric constant (ε∗) and ac electrical conductivity (σ_{ac}). Typically, the ε' and ε" are used to represent the real and imaginary components of the complex dielectric constant (ε∗) for MOS's. The real part, sometimes referred to as the relative permittivity or dielectric constant, is represented by ε'. It is a measure of the ability of the material to store electric charge in an electric field. ε" represents the imaginary part, which is also known as the dielectric loss factor. It is a measure of the energy that is lost as heat when the material is subjected to an electric field. The values of ε' and ε" for MOS's depend on factors such as the materials used in the MOS and the frequency of the applied electric field. The complex dielectric constant can be defined as follows equation;

$$\varepsilon^* = \varepsilon' - i\varepsilon'' \tag{4}$$

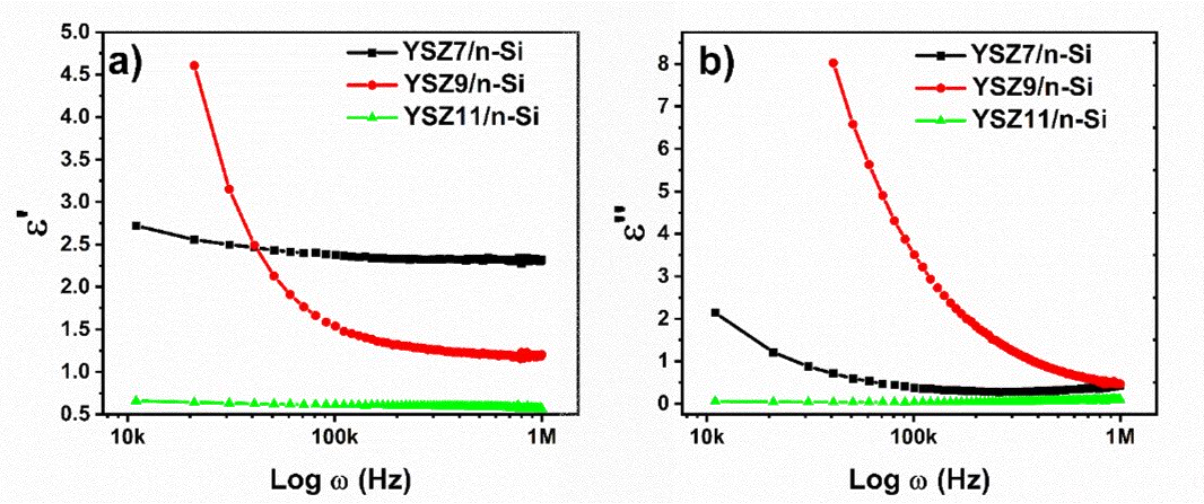

Figure 7. *(a) The plots of ε^'- log (ω) and (b) ε^''- log (ω) for Ag/YSZ/n-Si MOS structures*

This formulation can be stated as follows: given the admittance measurements,

$$\varepsilon^* = \frac{Y^*}{i\omega C_0} = \frac{C}{C_0} - i\frac{G}{\omega C_0} \tag{5}$$

where ω is the angular frequency of the applied electric field, and Y*, C, G, and C0 represent the measured admittance, capacitance, conductance, and capacitance of empty space of the dielectric material, respectively. Consequently, ε' and ε" can be expressed by the following equations:

$$\varepsilon' = \frac{C}{C_0} \qquad \varepsilon'' = \frac{G}{\omega C_0} \tag{6}$$

The frequency dependent ε^' and ε^" versus log (ω) are indicated in Figure 7 (a)-(b). When the graph is examined, it shows that ε and ε″ values are a strong function of frequency and that these values decrease with rising frequency. The decline in these values with frequency is usually attributed to the density of surface states, dipole, and interfacial polarization [50]. The loss tangent (tan δ) is a measure of the dielectric losses in a material, and it is commonly used to describe the electrical behavior of dielectric

materials. The ratio of the imaginary to real components of the dielectric constant is known as the loss tangent:

$$tan\ \delta\ = \frac{\varepsilon''}{\varepsilon'} \quad (7)$$

The term "loss tangent" refers to the process by which electrical energy dissipates within a dielectric material as a result of internal mechanisms that transform electrical energy into heat or other types of energy. Other examples of these mechanisms include electronic polarization, dipole relaxation, and molecular rotations. Furthermore, because the loss tangent is a frequency-dependent metric, it changes depending on the frequency of the electrical field that is being applied. Molecular and dipole rotations are frequently the dominant phenomena in the loss tangent at high frequencies, whereas electronic polarization predominates at low frequencies. Figure 8 (a) demonstrates the tan δ versus log (ω) for fabricated MOS structures. The loss tangent is an important parameter for dielectric materials because it affects the performance of various electrical devices, such as capacitors, transmission lines, and antennas [51]. High loss tangent materials are typically used in applications where energy dissipation is desired, such as in damping materials, while low loss tangent materials are preferred for applications where energy conservation is important, such as in high-Q resonators or microwave components [51]. There are not many studies in the literature examining the effect of deposition temperature on the dielectric properties of thin films on Si substrates. One of these few researches is the study conducted by Mehraj et al. [52], which examined the effect of annealing temperature on SnO_2. They reported that the peak in the tan δ graph occurs at high frequencies and that the jumping speed of charged particles (e−) increases as the annealing temperature increases. The Rezlescu model [53] provides a well-explained reasoning for the increased intensity of relaxation peak with annealing temperature. Based on this model, the relaxation peaks are a result of the combined contribution of n-type and p-type charge carriers [54]. Another important parameter for MOS structures is the AC electrical conductivity (σ_AC). The σ_AC is a complex quantity that describes the ability of a dielectric material to conduct AC current under the influence of an electric field. The expression for the AC electrical conductivity is:

$$\sigma_{AC}\ = \varepsilon''\omega\varepsilon_0 \quad (8)$$

Here ε_0 is the permittivity of free space. The variation in AC conductivity with frequency for Ag/YSZ/n-Si MOS at room temperature is presented in Figure 8 (b). The figure shows that the AC conductivity of the structures exhibits frequency-dependent behavior, and an increase in AC conductivity is observed with the increase in frequency. The observed increase in AC conductivity may be due to an improvement in the conduction process at a specific temperature within the high frequency range [55].

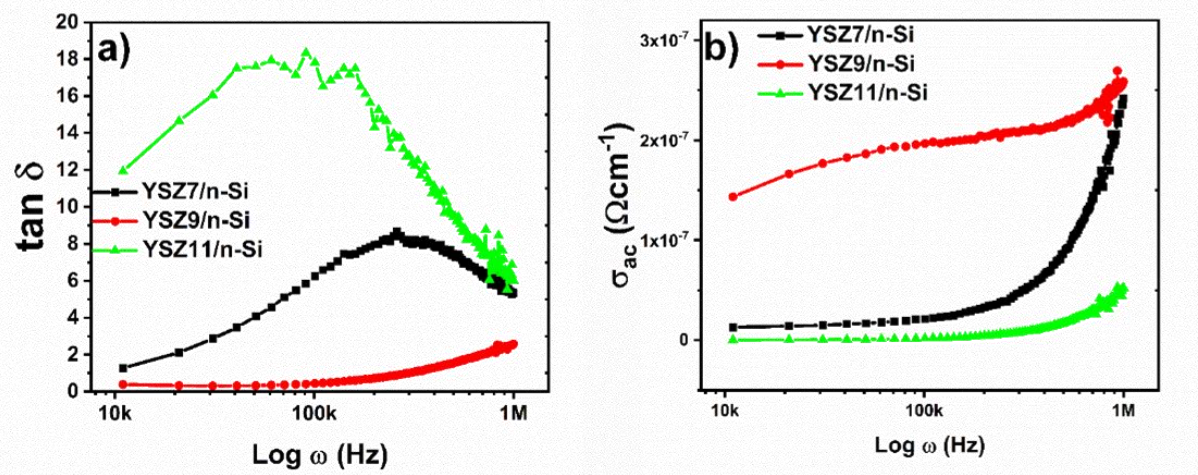

Figure 8. (a) *The plots of tan δ- log (ω) and* ***(b)*** σ_{AC}*- log (ω) for Ag/YSZ/n-Si MOS structures*

Conclusion

The yttrium-stabilized zirconia thin films were successfully grown at different deposition temperatures by sol-gel spin-coating technique. XRD analysis of YSZ films with thicknesses ranging from 95 to 220 nm showed that the cubic phase peaks were prominent and their intensities increased with higher deposition temperature. The XRD analysis also identified the crystallite sizes, dislocation density and microstrain of the thin films. It was observed that the crystal size of the YSZ thin films increased from 16 nm to 22 nm with increasing deposition temperature. AFM measurements showed that the surface roughness of the thin films changed with the deposition temperature, increasing from 7.72 nm to 11.92 nm. The optical transmittance of the YSZ thin films was investigated over a wavelength range of 200-900 nm, including both visible and near infrared spectra. The results showed a slight increase in optical transmittance with higher deposition temperature. Finally, MOS devices were fabricated using the YSZ films to evaluate their dielectric properties. The dielectric parameters of the Ag/YSZ/n-Si MOS structures were strongly dependent on frequency, including capacitance, conductivity and other related properties.

Acknowledgement We would like to thank Dr. Canan Aytug Ava for her contribution to the acquisition of AFM images. Batman University Commission of Scientific Research Project under Grant No. BTUBAP-2024-SHMYO-01 provided support for this study.

Funding/Financial Disclosure Not applicable.

Ethics Committee Approval and Permissions The study does not require ethics committee approval or any special permission.

Conflicts of Interest The authors declare that they have no known competing financial interests or personal relationships that could have appeared to influence the work reported in this paper.

Authors Contribution The author contributions to this article are as follows: Veysel Eratilla, Discussion, Editing and interpretation, Serif Ruzgar, Thin film deposition and MOS fabrication, Electrical and Optical measurements, Data analyses and graphs, Discussion, interpretation, Writing and editing.

References

[1] Piconi, C., & Maccauro, G. (1999). Zirconia as a ceramic biomaterial. *Biomaterials, 20*(1), 1-25. https://doi.org/10.1016/S0142-9612(98)00010-6

[2] Sprio, S., Guicciardi, S., Bellosi, A., & Pezzotti, G. (2006). Yttria-stabilized zirconia films grown by radiofrequency magnetron sputtering: Structure, properties and residual stresses. *Surface and Coatings Technology, 200*(14), 4579-4585. https://doi.org/10.1016/j.surfcoat.2005.04.003

[3] Kumar, D., Singh, A., Saini, B. S., Choudhary, B. C., Shinde, V., & Kaur, R. (2021). Effect of Ni doping on the structural and optical properties of ZrO_2 thin films. *Journal of Electronic Materials, 50*(1), 65-74. https://doi.org/10.1007/s11664-020-08558-0

[4] Kandpal, K., Gupta, N., Singh, J., & Shekhar, C. (2020). On the threshold voltage and performance of ZnO-based thin-film transistors with a ZrO_2 gate dielectric. *Journal of Electronic Materials, 49*(5), 3156-3164. https://doi.org/10.1007/s11664-020-08055-4

[5] Van, H. N., Van Huan, P., Nguyen, D.-H., Vu, N. H., & Pham, V.-H. (2019). Up/down-conversion luminescence of Er_3+ doped $ZrO_2 \cdot Al_2O_3$ powder. *Journal of Electronic Materials, 48*(12), 8054-8060. https://doi.org/10.1007/s11664-019-07644-2

[6] Kumar, D., Singh, A., Kaur, N., Thakur, A., & Kaur, R. (2020). Tailoring structural and optical properties of ZrO_2 with nickel doping. *SN Applied Sciences, 2*(4), 644. https://doi.org/10.1007/s42452-020-2491-z

[7] Chevalier, J. (2006). What future for zirconia as a biomaterial? *Biomaterials, 27*(4), 535-543. https://doi.org/10.1016/j.biomaterials.2005.07.034

[8] Chen, L. B. (2006). Yttria-stabilized zirconia thermal barrier coatings-A review. *Surface Review and Letters, 13*(05), 535-544. https://doi.org/10.1142/S0218625X06008670

[9] Guo, X., Vasco, E., Mi, S., Szot, K., Wachsman, E., & Waser, R. (2005). Ionic conduction in zirconia films of nanometer thickness. *Acta Materialia, 53*(19), 5161-5166. https://doi.org/10.1016/j.actamat.2005.07.033

[10] Flinn, B. D., deGroot, D. A., Mancl, L. A., & Raigrodski, A. J. (2012). Accelerated aging characteristics of three yttria-stabilized tetragonal zirconia polycrystalline dental materials. *The Journal of Prosthetic Dentistry, 108*(4), 223-230. https://doi.org/10.1016/S0022-3913(12)60166-8

[11] Cano, F. J., Castilleja-Escobedo, O., Espinoza-Pérez, L. J., Reynosa-Martínez, C., & Lopez-Honorato, E. (2021). Effect of deposition conditions on phase content and mechanical properties of yttria-stabilized zirconia thin films deposited by sol-gel/dip-coating. *Journal of Nanomaterials*, e4449890. https://doi.org/10.1155/2021/4449890

[12] Guven, S., Beydemir, K., Dundar, S., & Eratilla, V. (2015). Evaluation of stress distributions in peri-implant and periodontal bone tissues in 3- and 5-unit tooth and implant-supported fixed zirconia restorations by finite elements analysis. *European Journal of Dentistry, 9*(3), 329-339. https://doi.org/10.4103/1305-7456.163223

[13] Eratilla, V., Yildiz, A. D., Guven, S., Eratilla, E. A., Karaman, T., Aguloglu, S., & Sumer, E. (2016). Measuring the resistance of different substructure materials by sticking them to dentine with two different resin cements in vitro. *Nigerian Journal of Clinical Practice, 19*(6). https://doi.org/10.4314/njcp.v19i6

[14] Zscherp, M. F., Glaser, J., Becker, C., Beyer, A., Cop, P., Schörmann, J., Volz, K., & Elm, M. T. (2020). Epitaxial growth and structural characterization of ceria deposited by atomic layer deposition on high-surface porous yttria-stabilized zirconia thin films. *Crystal Growth & Design, 20*(4), 2194-2201. https://doi.org/10.1021/acs.cgd.9b01112

[15] Liu, C.-F., Tang, X.-G., Guo, X.-B., Liu, Q.-X., Jiang, Y.-P., Tang, Z.-H., & Li, W.-H. (2020). Photodiode characteristics of HfO_2 thin films prepared by magnetron sputtering. *Materials & Design, 188,* 108465. https://doi.org/10.1016/j.matdes.2019.108465

[16] Liu, C. W., Liu, W. T., Lee, M. H., Kuo, W. S., & Hsu, B. C. (2000). A novel photodetector using MOS tunneling structures. *IEEE Electron Device Letters, 21*(6), 307-309. https://doi.org/10.1109/55.843159

[17] Çokduygulular, E., Çetinkaya, Ç., Yalçın, Y., & Kınacı, B. (2020). A comprehensive study on Cu-doped ZnO (CZO) interlayered MOS structure. *Journal of Materials Science: Materials in Electronics, 31*(16), 13646-13656. https://doi.org/10.1007/s10854-020-03922-6

[18] Jang, D. Y., Kim, H. K., Kim, J. W., Bae, K., Schlupp, M. V. F., Park, S. W., Prestat, M., & Shim, J. H. (2015). Low-temperature performance of yttria-stabilized zirconia prepared by atomic layer deposition. *Journal of Power Sources, 274,* 611-618. https://doi.org/10.1016/j.jpowsour.2014.10.022

[19] Ouyang, Z., Meng, L., Raman, P., Cho, T. S., & Ruzic, D. N. (2011). Laser-assisted plasma coating at atmospheric pressure: Production of yttria-stabilized zirconia thermal barriers. *Journal of Physics D: Applied Physics, 44*(26), 265202. https://doi.org/10.1088/0022-3727/44/26/265202

[20] Sønderby, S., Aijaz, A., Helmersson, U., Sarakinos, K., & Eklund, P. (2014). Deposition of yttria-stabilized zirconia thin films by high power impulse magnetron sputtering and pulsed magnetron sputtering. *Surface and Coatings Technology, 240,* 1-6. https://doi.org/10.1016/j.surfcoat.2013.12.001

[21] Schlupp, M. V. F., Prestat, M., Martynczuk, J., Rupp, J. L. M., Bieberle-Hütter, A., & Gauckler, L. J. (2012). Thin film growth of yttria stabilized zirconia by aerosol assisted chemical vapor deposition. *Journal of Power Sources, 202,* 47-55. https://doi.org/10.1016/j.jpowsour.2011.11.016

[22] Díaz-Parralejo, A., Macías-García, A., Sánchez-González, J., Díaz-Díez, M. Á., & Cuerda-Correa, E. M. (2011). A novel strategy for the preparation of yttria-stabilized zirconia powders: Deposition and scratching of thin films obtained by the sol–gel method. *Journal of Non-Crystalline Solids, 357*(3), 1090-1095. https://doi.org/10.1016/j.jnoncrysol.2010.10.025

[23] Courtin, E., Boy, P., Rouhet, C., Bianchi, L., Bruneton, E., Poirot, N., Laberty-Robert, C., & Sanchez, C. (2012). Optimized sol–gel routes to synthesize yttria-stabilized zirconia thin films as solid electrolytes for solid oxide fuel cells. *Chemistry of Materials, 24*(23), 4540-4548. https://doi.org/10.1021/cm302177s

[24] Pakma, O., Özdemir, C., Kariper, İ. A., Özaydın, C., & Güllü, Ö. (2016). Wet chemical methods for producing mixing crystalline phase ZrO_2 thin film. *Applied Surface Science, 377,* 159-166. https://doi.org/10.1016/j.apsusc.2016.03.107

[25] Mathew Simon, S., George, G., M s, S., V p, P., Anna Jose, T., Vasudevan, P., Saritha, A. C., Biju, P. R., Joseph, C., & Unnikrishnan, N. V. (2021). Recent advancements in multifunctional applications of sol-gel derived polymer incorporated TiO_2-ZrO_2 composite coatings: A comprehensive review. *Applied Surface Science Advances, 6,* 100173. https://doi.org/10.1016/j.apsadv.2021.100173

[26] Shao, Z., Zhou, W., & Zhu, Z. (2012). Advanced synthesis of materials for intermediate-temperature solid oxide fuel cells. *Progress in Materials Science, 57*(4), 804-874. https://doi.org/10.1016/j.pmatsci.2011.08.002

[27] Waghmare, M., Sonone, P., Patil, P., Kadam, V., Pathan, H., & Ubale, A. (2018). Spray pyrolytic deposition of zirconium oxide thin films: influence of concentration on structural and optical properties. *Engineered Science, 5*(2), 79-87.

[28] Rusli, N. A., Muhammad, R., Ghoshal, S. K., Nur, H., & Nayan, N. (2020). Annealing temperature induced improved crystallinity of YSZ thin film. *Materials Research Express, 7*(5), 056406. https://doi.org/10.1088/2053-1591/ab9039

[29] Ramos-Guerra, A. I., Guzmán-Mendoza, J., García-Hipólito, M., Alvarez-Fregoso, O., & Falcony, C. (2015). Multicolored photoluminescence and structural properties of zirconium oxide films co-doped with Tb3+ and Eu3+ ions. *Ceramics International, 41*(9, Part A), 11279-11286. https://doi.org/10.1016/j.ceramint.2015.05.084

[30] Malek, M. F., Mamat, M. H., Musa, M. Z., Khusaimi, Z., Sahdan, M. Z., Suriani, A. B., Ishak, A., Saurdi, I., Rahman, S. A., & Rusop, M. (2014). Thermal annealing-induced formation of ZnO nanoparticles: Minimum strain and stress ameliorate preferred c-axis orientation and crystal-growth properties. *Journal of Alloys and Compounds, 610,* 575-588. https://doi.org/10.1016/j.jallcom.2014.05.036

[31] Aksoy, S., & Caglar, Y. (2014). Structural transformations of TiO_2 films with deposition temperature and electrical properties of nanostructure n-TiO_2/p-Si heterojunction diode. *Journal of Alloys and Compounds, 613,* 330-337. https://doi.org/10.1016/j.jallcom.2014.05.192

[32] Hu, S. Y., Lee, Y. C., Lee, J. W., Huang, J. C., Shen, J. L., & Water, W. (2008). The structural and optical properties of ZnO/Si thin films by RTA treatments. *Applied Surface Science, 254*(6), 1578-1582. https://doi.org/10.1016/j.apsusc.2007.07.134

[33] Heiroth, S., Frison, R., Rupp, J. L. M., Lippert, T., Barthazy Meier, E. J., Müller Gubler, E., Döbeli, M., Conder, K., Wokaun, A., & Gauckler, L. J. (2011). Crystallization and grain growth characteristics of yttria-stabilized zirconia thin films grown by pulsed laser deposition. *Solid State Ionics, 191*(1), 12-23. https://doi.org/10.1016/j.ssi.2011.04.002

[34] Cai, H., Tuokedaerhan, K., Lu, Z., Zhang, R., & Du, H. (2022). Effect of annealing temperature on the structural, optical, and electrical properties of al-doped ZrO_2 gate dielectric films treated by the sol–gel method. *Coatings, 12*(12). https://doi.org/10.3390/coatings12121837

[35] Fan, C., Liu, A., Meng, Y., Guo, Z., Liu, G., & Shan, F. (2017). Solution-processed SrOx-gated oxide thin-film transistors and inverters. *IEEE Transactions on Electron Devices, 64*(10), 4137-4143. https://doi.org/10.1109/TED.2017.2742060

[36] Tilli, M., Paulasto-Krockel, M., Motooka, T., Lindroos, V., Airaksinen, V.-M., Franssila, S., & Lehto, A. (2009). Handbook of Silicon Based MEMS Materials and Technologies. Elsevier.

[37] Wang, C. (2021). Effect of annealing temperature on the structure and optical properties of Mn doped ZnS thin films. *Journal of Modern Optics, 68*(14), 771-775. https://doi.org/10.1080/09500340.2021.1946183

[38] Li, J., Yang, W., Su, J., & Yang, C. (2018). Effects of deposition temperature on structural, optical properties and laser damage of laTiO$_3$ thin films. *Advances in Condensed Matter Physics,* e7328429. https://doi.org/10.1155/2018/7328429

[39] Hojabri, A. (2016). Structural and optical characterization of ZrO_2 thin films grown on silicon and quartz substrates. *Journal of Theoretical and Applied Physics, 10*(3), 219-224. https://doi.org/10.1007/s40094-016-0218-8

[40] Bakacak, P. K., Gur, E., Bayram, O., Tuzemen, S., & Simsek, O. (2021). Photoluminescence and structural properties of zirconium dioxide thin films produced by RF sputtering technique. *Journal of Materials Science: Materials in Electronics, 32*(6), 7541-7549. https://doi.org/10.1007/s10854-021-05468-7

[41] Satoh, N., Nakashima, T., Kamikura, K., & Yamamoto, K. (2008). Quantum size effect in TiO_2 nanoparticles prepared by finely controlled metal assembly on dendrimer templates. *Nature Nanotechnology, 3*(2). https://doi.org/10.1038/nnano.2008.2

[42] Gu, P., Zhu, X., & Yang, D. (2019). Effect of annealing temperature on the performance of photoconductive ultraviolet detectors based on ZnO thin films. *Applied Physics A, 125*(1), 50. https://doi.org/10.1007/s00339-018-2361-3

[43] Murarka, S. P., Eizenberg, M., & Sinha, A. K. (2003). Interlayer Dielectrics for Semiconductor Technologies. Elsevier.

[44] Özdemir, M. C., Sevgili, Ö., Orak, İ., & Türüt, A. (2020). Arayüzey doğal oksit tabakalı Al/p-Si/Al yapıların dielektrik karakteristiklerine ölçüm frekansının etkileri. *Journal of the Institute of Science and Technology, 10*(1). https://doi.org/10.21597/jist.612518

[45] Yıldız, D. E., & Dökme, İ. (2011). Frequency and gate voltage effects on the dielectric properties and electrical conductivity of Al/SiO_2/p-Si metal-insulator-semiconductor Schottky diodes. *Journal of Applied Physics, 110*(1), 014507-014507-5. https://doi.org/10.1063/1.3602090

[46] Cavdar, S., Demirolmez, Y., Turan, N., Koralay, H., & Tuğluoğlu, N. (2022). Analysis of voltage and frequency-dependent series resistance and interface states of Al/$ZnCo_2O_4$: Gelatin/n-Si diode. *Journal of Materials Science: Materials in Electronics, 33*(29), 22932-22940. https://doi.org/10.1007/s10854-022-09063-2

[47] Lok, R., Budak, E., & Yilmaz, E. (2020). Structural characterization and electrical properties of Nd_2O_3 by sol–gel method. *Journal of Materials Science: Materials in Electronics, 31*(4), 3111-3118. https://doi.org/10.1007/s10854-020-02857-2

[48] Elgazzar, E., Tataroğlu, A., Al-Ghamdi, A. A., Al-Turki, Y., Farooq, W. A., El-Tantawy, F., & Yakuphanoglu, F. (2016). Thermal sensors based on delafossite film/p-silicon diode for low-temperature measurements. *Applied Physics A, 122*(6), 617. https://doi.org/10.1007/s00339-016-0148-y

[49] Gullu, H. H., Yildiz, D. E., Surucu, O., & Parlak, M. (2020). Frequency effect on electrical and dielectric characteristics of HfO_2-interlayered Si-based Schottky barrier diode. *Journal of Materials Science: Materials in Electronics, 31*(12), 9394-9407. https://doi.org/10.1007/s10854-020-03479-4

[50] Pirgholi-Givi, G., Altındal, Ş., Shahedi Asl, M., Sabahi Namini, A., Farazin, J., & Azizian-Kalandaragh, Y. (2021). The effect of cadmium impurities in the (PVP–TeO_2) interlayer in Al/p-Si (MS) Schottky barrier diodes (SBDs): Exploring its electrophysical parameters. *Physica B: Condensed Matter, 604,* 412617. https://doi.org/10.1016/j.physb.2020.412617

[51] Sebastian, M. T. (2010). Dielectric Materials for Wireless Communication. Elsevier.

[52] Mehraj, S., Ansari, M. S., & Alimuddin. (2015). Annealed SnO_2 thin films: Structural, electrical and their magnetic properties. *Thin Solid Films, 589,* 57-65. https://doi.org/10.1016/j.tsf.2015.04.065

[53] Rezlescu, N., & Rezlescu, E. (1974). Dielectric properties of copper containing ferrites. *Physica Status Solidi (a), 23*(2), 575-582. https://doi.org/10.1002/pssa.2210230229

[54] Jonscher, A. K. (1999). Dielectric relaxation in solids. *Journal of Physics D: Applied Physics, 32*(14), R57. https://doi.org/10.1088/0022-3727/32/14/201

[55] Shukla, N., & Dwivedi, D. K. (2016). Dielectric relaxation and AC conductivity studies of Se90Cd10−xInx glassy alloys. *Journal of Asian Ceramic Societies*, *4*(2), 178-184. https://doi.org/10.1016/j.jascer.2016.02.003